

Adaptive Scaling of Policy Constraints for Offline Reinforcement Learning

Tan Jing¹, Xiaorui Li², Chao Yao², Xiaojuan Ban², Yuetong Fang¹, Renjing Xu^{1*}, Zhaolin Yuan^{2*}

¹ Hong Kong University of Science and Technology (Guangzhou), China

² University of Science and Technology Beijing, China

Emails: renjingxu@hkust-gz.edu.cn, yuanzhaolin@ustb.edu.cn

Abstract

Offline reinforcement learning (RL) enables learning effective policies from fixed datasets without any environment interaction. Existing methods typically employ policy constraints to mitigate the distribution shift encountered during offline RL training. However, because the scale of the constraints varies across tasks and datasets of differing quality, existing methods must meticulously tune hyperparameters to match each dataset, which is time-consuming and often impractical. We propose Adaptive Scaling of Policy Constraints (ASPC), a second-order differentiable framework that dynamically balances RL and behavior cloning (BC) during training. We theoretically analyze its performance improvement guarantee. In experiments on 39 datasets across four D4RL domains, ASPC using a single hyperparameter configuration outperforms other adaptive constraint methods and state-of-the-art offline RL algorithms that require per-dataset tuning while incurring only minimal computational overhead. The code will be released at <https://github.com/Colin-Jing/ASPC>.

1 Introduction

Offline reinforcement learning (RL) learns a policy exclusively from a fixed, pre-collected dataset without further interactions with the environment (Levine et al. 2020). This characteristic is particularly crucial in real-world applications such as autonomous driving (El Sallab et al. 2017; Kendall et al. 2019), healthcare (Prasad et al. 2017; Wang et al. 2018), industry (Zhan et al. 2022; Yuan et al. 2024), and other tasks, where interacting with the environment can be expensive and risky. Thus, offline RL holds considerable practical significance in addressing real-world decision-making challenges.

Despite the potential advantages, a critical challenge in offline RL is the distribution shift (Levine et al. 2020) between the offline data and the training policies, often leading to suboptimal or even invalid policy updates. Many methods have been proposed to mitigate the adverse effects of the distribution shift. A common strategy is to impose explicit or implicit policy constraints, ensuring that the learned policy remains close to the behavior policy used to collect the dataset. By imposing constraints on policy updates, these methods can effectively mitigate the extrapolation error of the Q value induced by the distribution shift while offering certain performance guarantees.

*Corresponding author

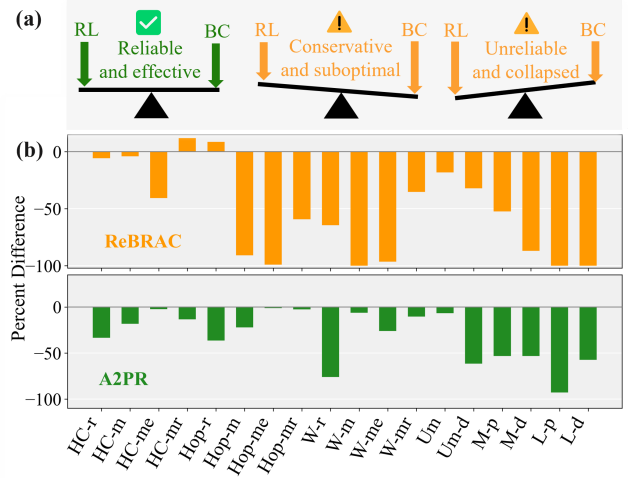


Figure 1: (a) The RL–BC trade-off in offline RL. ASPC dynamically balances RL and BC, yielding a reliable and effective policy (left). Existing methods fail to properly calibrate this trade-off, resulting in suboptimal or collapsed policies (middle and right). (b) Percent difference in performance for ReBRAC and A2PR under a single hyperparameter setting across all datasets. HC = HalfCheetah, Hop = Hopper, W = Walker, r = random, m = medium, mr = medium-replay, me = medium-expert, Um = umaze, M = medium, L = large, d = diverse, p = play. Large drops highlight the sensitivity of prior methods to per-dataset tuning.

However, despite the promise of policy constraint methods, a key limitation is that the scale of the policy constraint often varies between datasets of different quality and between tasks. In practice, many methods, regardless of whether their core innovation is the adaptive policy constraint, rely on different hyperparameter settings to adjust the scale for each dataset to achieve optimal performance (Chen et al. 2023; Yang et al. 2023; Tarasov et al. 2024a; Liu et al. 2024). However, in offline RL tasks, such exhaustive hyperparameter tuning is often prohibitively expensive or outright infeasible in critical applications. If a fixed hyperparameter setting is applied across different datasets, the algorithm struggles to achieve strong performance. For example, as shown in Figure 1(b), when a single configuration is applied to all datasets, the per-

formance of ReBRAC (Tarasov et al. 2024a) and A2PR (Liu et al. 2024) suffers a severe degradation. There are also adaptive policy constraint approaches that use fixed hyperparameters; however, they center on locally re-weighting the policy toward higher-value actions and ignore the global trade-off scale between the RL objective and the behavior cloning (BC) constraint. As a result, their performance still lags behind that of methods whose hyperparameters are painstakingly tuned for each dataset (Peng et al. 2023; Yang et al. 2024).

To enable a single hyperparameter configuration to match or exceed the performance of finely tuned methods across datasets of varying quality and tasks, we propose an adaptive scaling of policy constraints (ASPC) approach that dynamically adjusts the constraint scale during training. The intuition of this method is shown in Figure 1(a). Our approach leverages a second-order differentiable optimization framework (Finn, Abbeel, and Levine 2017) to balance the goals of RL and BC. Specifically, we parameterize the scale factor α as a learnable parameter that balances the RL objective \mathcal{L}_{RL} and the BC objective \mathcal{L}_{BC} in TD3+BC (Fujimoto and Gu 2021). The combined objective \mathcal{L} is given by

$$\mathcal{L} = \alpha \mathcal{L}_{\text{RL}} + \mathcal{L}_{\text{BC}}, \quad (1)$$

For the full definitions of α , refer to Eq. (3) and Eq. (4). During training, α is dynamically adjusted by constraining the rate of change of the Q-value and the BC loss, enabling the algorithm to discover a more stable learning path and exhibit remarkable adaptability across tasks and datasets.

We theoretically analyze the performance improvement guarantee of ASPC and extensively evaluate it on the D4RL benchmark (Levine et al. 2020), covering four domains: MuJoCo, Maze2d, AntMaze and Adroit across nine tasks and 39 datasets of varying quality. Our empirical results demonstrate that ASPC not only outperforms other adaptive policy constraint methods but also exceeds the performance of state-of-the-art offline RL algorithms that depend on meticulously tuned hyperparameters for each dataset, while adding only minimal computational overhead to the original TD3+BC backbone.

2 Related Works

2.1 Offline RL

Offline RL aims to learn policies purely from static datasets and suffers from distribution shift between the data-collecting behavior policy and the learned policy, leading to value overestimation and policy collapse. Policy constraint methods explicitly (Fujimoto, Meger, and Precup 2019; Fujimoto and Gu 2021) or implicitly (Kumar et al. 2020; Kostrikov, Nair, and Levine 2022) regularize the target policy toward the behavior distribution to mitigate this shift. Uncertainty-aware approaches estimate model or value uncertainty and penalize high-uncertainty actions (An et al. 2021; Bai et al. 2022; Zhang et al. 2023). Sequence modeling methods recast RL as conditional sequence prediction over state-action-return trajectories using transformer architectures (Chen et al. 2021; Janner, Li, and Levine 2021). Model-based techniques learn dynamic models for pessimistic planning or conservative rollouts (Yu et al. 2020; Kidambi et al. 2020; Yu et al. 2021). In this paper, we focus on the policy constraint methods.

2.2 Adaptive Policy Constraint

Adaptive policy-constraint methods aim to automatically tailor the strength of policy regularization to the characteristics of each offline dataset. AW (Hong et al. 2023) up-weights higher-return trajectories, tightening regularization around the most reliable transitions. wPC (Peng et al. 2023) imposes stricter constraints on high-value actions and relaxes them on low-value ones. OAP (Yang et al. 2023) queries a black-box expert for action preferences to dynamically modulate constraint strength. PRDC (Ran et al. 2023) locates the nearest state-action pair in the dataset and applies a soft constraint toward that action, offering flexible regularization. GORL (Yang et al. 2024) trains a guiding network on extra expert demonstrations to predict sample-level constraint intensities, enabling fine-grained adaptation. A2PR (Liu et al. 2024) leverages a VAE-enhanced behavior policy to propose high-advantage actions, guiding the learner toward better moves while still restricting out-of-distribution actions. IEPC (Liu and Hofert 2024) combines a GAN-based implicit action-matching constraint with an explicit advantage weight, adaptively steering the policy toward reliable in-dataset regions. However, these methods either require per-dataset hyperparameter search or apply a fixed configuration that yields only limited improvements. In contrast, our ASPC method delivers robust performance across diverse datasets using a single hyperparameter set.

3 Preliminaries

RL problems are formulated as a Markov decision process (MDP), described by the tuple (S, A, P, R, γ) . The set of states is S , the set of actions is A , the transition probability function is $P(s'|s, a)$, the reward function is $R(s, a)$, and $\gamma \in [0, 1]$ is the discount factor. The objective is to find a policy $\pi : S \rightarrow A$ that maximizes the expected discounted return. This objective is equivalently expressed as maximizing the Q-value $Q^\pi(s, a)$ under π , given by:

$$Q^\pi(s, a) = \mathbb{E}_\pi \left[\sum_{t=0}^{\infty} \gamma^t R(s_t, a_t) \mid s_0 = s, a_0 = a \right], \quad (2)$$

where s_t and a_t represent the state and action at time t . In practice, RL algorithms update Q-values using the Bellman equation as an iterative rule, seeking to converge to the optimal policy π^* .

A central challenge for offline RL is the distribution shift: when a state-action pair (s, a) lies outside the dataset \mathcal{D} , directly optimizing the Q-function may cause severe overestimation. One remedy is to constrain the target policy π to stay close to the behaviour policy π_β . TD3+BC (Fujimoto and Gu 2021) does so by solving:

$$\pi = \arg \max_{\pi} \mathbb{E}_{(s, a) \sim \mathcal{D}} \left[\lambda \underbrace{Q(s, \pi(s))}_{\text{RL}} - \underbrace{(\pi(s) - a)^2}_{\text{BC}} \right], \quad (3)$$

where the weighting coefficient

$$\lambda = \frac{\alpha}{\frac{1}{N} \sum_i |Q(s_i, a_i)|} \quad (4)$$

normalizes the RL term to the scale of the BC loss. In vanilla TD3+BC, α is fixed and the denominator is computed with $\text{detach}(Q(s_i, a_i))$, so λ is treated as a constant during backpropagation. Instead of keeping the scale factor α static, we update it throughout training.

4 Method

In this section, we give a comprehensive overview of the ASPC algorithm. Section 4.1 introduces its second-order differentiable optimization framework, which dynamically balances the RL and BC objectives. Section 4.2 details the implementation based on TD3+BC. Section 4.3 presents a theoretical analysis of the framework, covering the symmetric regularization term and performance improvement analysis.

4.1 Adaptive Scaling of Policy Constraints

To adaptively adjust the relative scaling between the RL and BC objectives, ASPC adopts a meta-learning approach (Finn, Abbeel, and Levine 2017; Franceschi et al. 2018). It turns the scale factor α in Eq. (4) into a learnable parameter and optimizes it dynamically via bilevel training, using inner update and outer update to maximize RL exploration near the behavior policy.

Inner Update Given the offline dataset $\mathcal{D} = \{(s, a)\}$, we adopt the TD3+BC objective

$$\mathcal{L}_{\text{inner}}(\theta; \alpha) = \mathbb{E}_{(s, a) \sim \mathcal{D}} \left[-\lambda Q(s, \pi_\theta(s)) + \|\pi_\theta(s) - a\|^2 \right], \quad (5)$$

where $\lambda = \alpha / (\frac{1}{N} \sum_{s_i \sim \mathcal{D}} |Q(s_i, \pi_\theta(s_i))|)$. We perform the gradient descent step

$$\tilde{\theta}(\alpha) = \theta - \eta_\theta \frac{\partial \mathcal{L}_{\text{inner}}(\theta; \alpha)}{\partial \theta}, \quad (6)$$

and regard $\tilde{\theta}(\alpha)$ as the output of the inner update. η_θ is the learning rate of θ . In practice, the update is kept differentiable with TorchOpt (Ren* et al. 2023).

Outer Update After the inner update we obtain parameters $\tilde{\theta}(\alpha)$ and construct three criteria:

$$\mathcal{L}_1 = -(\alpha \cdot \text{detach}) \cdot \frac{\bar{Q}_{t+1}}{|\bar{Q}|_{t+1}} + L_{t+1}^{\text{BC}}, \quad (7)$$

$$\mathcal{L}_2 = (\text{EMA}[\bar{Q}_{t+1}] - \text{EMA}[\bar{Q}_t])^2, \quad (8)$$

$$\mathcal{L}_3 = (\mathcal{L}_2 \cdot \text{detach}) \cdot c_\infty^2 \Delta L_\infty^{\text{BC}}, \quad (9)$$

where the components are defined as:

$$\begin{aligned} \bar{Q}_{t+1} &:= \mathbb{E}_{s \sim \mathcal{D}}[Q(s, \pi_{\tilde{\theta}}(s))], \\ |\bar{Q}|_{t+1} &:= \mathbb{E}_{s \sim \mathcal{D}}[|Q(s, \pi_{\tilde{\theta}}(s))|], \\ L_{t+1}^{\text{BC}} &:= \mathbb{E}_{(s, a) \sim \mathcal{D}}[\|\pi_{\tilde{\theta}}(s) - a\|^2], \\ c_\infty^2 &:= \sup_{(s, a) \in \mathcal{D}} \|\pi_t(s) - a\|^2, \\ \Delta L_\infty^{\text{BC}} &:= \sup_{(s, a) \in \mathcal{D}} |\|\pi_{t+1}(s) - a\|^2 - \|\pi_t(s) - a\|^2|. \end{aligned}$$

We denote by t the index of inner updates, and by $t + 1$ the outer iteration that follows. $\cdot \text{detach}$ indicates to stop its backpropagation. The exponential moving average $\text{EMA}[\cdot]$ smooths Q-values across iterations. \bar{Q}_{t+1} , L_{t+1}^{BC} and $\Delta L_\infty^{\text{BC}}$ carry gradients. The outer objective is the sum of the three terms,

$$\mathcal{L}_{\text{outer}}(\tilde{\theta}(\alpha)) = \mathcal{L}_1 + \mathcal{L}_2 + \mathcal{L}_3. \quad (10)$$

Remark 4.1 (On the constant w in \mathcal{L}_3). Theorem 4.5 and its proof A.3 indicate that \mathcal{L}_3 should be multiplied by a constant w . For simplicity and to eliminate extra tuning, we set $w = 1$ throughout and achieve competitive results.

To update α , we treat the inner update parameters $\tilde{\theta}(\alpha)$ as an implicit function of α and use second-order derivatives. Let η_α be the learning rate of α . The gradient-descent step is

$$\alpha \leftarrow \alpha - \eta_\alpha \left(\frac{\partial \mathcal{L}_{\text{outer}}(\tilde{\theta}(\alpha))}{\partial \tilde{\theta}} \frac{\partial \tilde{\theta}(\alpha)}{\partial \alpha} \right), \quad (11)$$

The outer loss has three coordinated components. \mathcal{L}_1 mirrors TD3+BC and steers α toward an improved RL-BC balance. \mathcal{L}_2 damps abrupt increases in the expected Q-value, whereas \mathcal{L}_3 curbs sudden shifts in BC loss, each stabilizing its respective term. Acting together, \mathcal{L}_2 and \mathcal{L}_3 adaptively moderate the step prescribed by \mathcal{L}_1 , preventing either objective from dominating, which could cause divergence or cap performance.

Algorithm 1: Adaptive Scaling of Policy Constraints

Initialize: critics Q_{ϕ_1}, Q_{ϕ_2} with targets $\bar{\phi}_{1,2}$, actor π_θ with target $\bar{\theta} \leftarrow \theta$, learnable parameter α , replay buffer \mathcal{D} ; update intervals k_π, k_α .

```

1: for  $i = 1$  to  $N$  do
2:   Critic update:
3:     Sample minibatch  $\{(s, a, r, s', d)\} \sim \mathcal{D}$ ;
4:     Compute TD targets  $y$  and update  $Q_{\phi_1}, Q_{\phi_2}$ 
5:   if  $i \bmod k_\pi = 0$  then
6:     Actor update (inner):
7:       Compute  $\mathcal{L}_{\text{inner}}(\theta; \alpha)$  by Eq. (5);
8:       Compute  $\tilde{\theta}(\alpha)$  by Eq. (6);
9:       Update actor:  $\theta \leftarrow \tilde{\theta}$ 
10:      if  $i \bmod (k_\pi \cdot k_\alpha) = 0$  then
11:        α update (outer):
12:        Compute  $\mathcal{L}_{\text{outer}}(\tilde{\theta}(\alpha))$  by Eq. (10);
13:        Update  $\alpha$  via Eq. (11)
14:      end if
15:      Soft update targets:
16:       $\bar{\phi}_{1,2} \leftarrow (1 - \tau)\bar{\phi}_{1,2} + \tau\phi_{1,2}$ ;
17:       $\bar{\theta} \leftarrow (1 - \tau)\bar{\theta} + \tau\theta$ 
18:    end if
19:  end for

```

4.2 Practical Implementation

This section details the concrete implementation of ASPC. Compared with the original TD3+BC algorithm, ASPC introduces only two modifications: (i) a redesigned critic network, and (ii) a learnable scale factor α . All other network

components and hyperparameters remain unchanged. See Appendix B.2 for a full specification.

Recent studies show that deeper critics (Kumar et al. 2022; Lee et al. 2022) and the insertion of LayerNorm between layers (Nikulin et al. 2023; Ball et al. 2023; Tarasov et al. 2024a) can mitigate Q-value over-estimation and improve stability. Following this evidence, we extend the TD3+BC critic from two to three hidden layers and insert a LayerNorm after each layer. An ablation of this choice is provided in Section 5.5.

Algorithm 1 lists the ASPC procedure. Blue highlights indicate lines that differ from the TD3+BC backbone. Although second-order gradients increase cost, we set the α -update interval k_α far longer than the actor-update interval k_π , which maintains performance while sharply reducing runtime. Section 5.4 analyses this trade-off in detail.

4.3 Theoretical Analysis

Assumption 4.2. The critic $Q(s, a)$ and the transition kernel $P(\cdot | s, a)$ are Lipschitz continuous in their action input. That is, there exist constants $L_Q, L_P > 0$ such that for all $s \in \mathcal{S}$ and all $a_1, a_2 \in \mathcal{A}$,

$$\|Q(s, a_1) - Q(s, a_2)\| \leq L_Q \|a_1 - a_2\|, \quad (12)$$

$$\|P(\cdot | s, a_1) - P(\cdot | s, a_2)\| \leq L_P \|a_1 - a_2\|. \quad (13)$$

Proposition 4.3 (Mutual bounds between ΔL_{BC} and $(\Delta Q)^2$). *Under Assumption 4.2, define $c = \sqrt{L_t^{BC}}$, $\Delta Q = \mathbb{E}_s [Q(s, \pi_{t+1}(s)) - Q(s, \pi_t(s))]$, $\Delta L_{BC} = |L_{t+1}^{BC} - L_t^{BC}|$. Then the following two inequalities hold:*

$$\Delta L_{BC} \geq \max \left\{ 2c \frac{|\Delta Q|}{L_Q} - \frac{(\Delta Q)^2}{L_Q^2}, 0, \frac{(\Delta Q)^2}{L_Q^2} - 2c \frac{|\Delta Q|}{L_Q} \right\}, \quad (14)$$

$$(\Delta Q)^2 \leq L_Q^2 (c + \sqrt{c^2 + \Delta L_{BC}})^2. \quad (15)$$

The detailed proof is provided in Appendix A.1. Proposition 4.3 shows that ΔQ provides a lower bound for ΔL_{BC} , while ΔL_{BC} provides an upper bound for $(\Delta Q)^2$. Thus either penalty partly enforces the other, but using both gives the strongest control. Some tasks perform well with a single term; others require both. Detailed results are in Section 5.5.

Proposition 4.4 (Single step performance lower bound). *For the update step from π_t to π_{t+1} define $\kappa := C L_P L_Q$. Then*

$$\begin{aligned} J(\pi_{t+1}) - J(\pi_t) &\geq \frac{1}{1-\gamma} \left(\Delta Q - \kappa [3c_\infty^2 \right. \\ &\quad \left. + 3c_\infty \sqrt{c_\infty^2 + \Delta L_\infty^{BC}} + \Delta L_\infty^{BC}] \right). \end{aligned} \quad (16)$$

The proof is provided in Appendix A.2.

Theorem 4.5 (Single step performance guarantee). *Assuming $\Delta L_\infty^{BC}/c_\infty^2 \ll 1$, the outer loss (10) guarantees*

$$J(\pi_{t+1}) - J(\pi_t) \geq 0. \quad (17)$$

The proof is provided in Appendix A.3.

Theorem 4.6 (Performance Gap to Optimal). *Let the warm-up stage produce an initial policy π_0 satisfying $L_{t_0}^{BC} \leq \varepsilon_0$. Assume further that $\max_s \|\pi^*(s) - \pi_\beta(s)\| \leq \varepsilon_\beta$ and that Algorithm 1 maintains a per-step improvement $J(\pi_{i+1}) - J(\pi_i) \geq \delta_{\min} > 0$ for every i . Then, for any horizon T ,*

$$J(\pi^*) - J(\pi_T) \leq \frac{C L_P R_{\max}}{1-\gamma} (\varepsilon_\beta + \sqrt{\varepsilon_0}) - T \delta_{\min}. \quad (18)$$

where C is a positive constant.

The proof is provided in Appendix A.4. Theorems 4.5 and 4.6 show that ASPC continually reduces the gap between the behavior policy π_β and the optimal policy π^* . By contrast, when α is held fixed, the single step gain $\delta_i = J(\pi_{i+1}) - J(\pi_i)$ either converges to zero too early or turns negative, leaving a substantial performance gap to the optimal policy.

5 Experiments

In this section we evaluate ASPC on the D4RL benchmark. Section 5.1 compares ASPC with strong baselines to demonstrate its adaptability and overall effectiveness. Section 5.2 analyzes the learning curves of α during training, further illustrating ASPC’s adaptive behaviour. Section 5.3 investigates the necessity of dynamically adjusting α . Section 5.4 reports runtime results to highlight the efficiency of ASPC. Section 5.5 presents ablation studies on the key components of ASPC.

5.1 Comparative Performance on Benchmark

We evaluate ASPC on 39 datasets spanning four D4RL domains (Levine et al. 2020): MuJoCo (v2), AntMaze (v2), Maze2d (v1), and Adroit (v1). Our baselines include TD3+BC (Fujimoto and Gu 2021) and IQL (Kostrikov, Nair, and Levine 2022) as standard policy-constraint methods. wPC (Peng et al. 2023) and A2PR (Liu et al. 2024) are state-of-the-art (SOTA) adaptive policy constraint methods built on TD3+BC. ReBRAC (Tarasov et al. 2024a) integrates multiple performance-boosting components into TD3+BC and has achieved SOTA results across a wide range of datasets. TD3+BC, wPC, A2PR, and ASPC are all set as the single hyperparameter set, whereas IQL and ReBRAC rely on dataset-specific hyperparameters found via grid search. We reproduce results for TD3+BC, wPC and A2PR. IQL and ReBRAC results are taken from (Tarasov et al. 2024a,b). Complete experimental details for each algorithm are provided in the appendix B.2.

The performance comparison is summarized in Table 1. ASPC achieves the best performance on MuJoCo and Maze2d, and exhibits competitive results on Adroit and AntMaze. Most notably, ASPC attains SOTA performance on average across all four domains, which not only outperforms other adaptive policy constraint methods but also surpasses approaches that rely on meticulous per-dataset hyperparameter tuning, highlighting its remarkable adaptability. Figure 2 makes this clear: the performance profile curves (left) place ASPC above all baselines for almost every threshold, and the min-max-scaled radar chart (right) gives ASPC the largest, most balanced polygon, visually confirming its strong and stable performance across tasks without per-dataset tuning.

Table 1: Average normalized score over the final evaluation across four random seeds. The best performance in each dataset is highlighted in **bold**, while the second-best performance is indicated with an underline. Blue shading indicates methods with top domain average performance. The symbol \pm denotes the standard deviation. \checkmark denotes fixed hyperparameters, whereas \times denotes dataset-specific ones. *To ensure fairness, TD3+BC and wPC employ the robust critic described in Section 5.5.

	Task Name	TD3+BC*(\checkmark)	A2PR(\checkmark)	IQL(\times)	wPC*(\checkmark)	ReBRAC(\times)	ASPC (Ours)(\checkmark)
HalfCheetah	Random	10.6 \pm 0.7	<u>21.1</u> \pm 0.8	19.5 \pm 0.8	18.8 \pm 0.7	29.5 \pm 1.5	20.8 \pm 0.9
	Medium	49.6 \pm 0.2	<u>56.1</u> \pm 0.3	50.0 \pm 0.2	54.8 \pm 0.2	65.6 \pm 1.0	<u>58.7</u> \pm 0.4
	Expert	100.4 \pm 0.4	99.9 \pm 3.2	95.5 \pm 2.1	103.8 \pm 2.4	105.9 \pm 1.7	<u>105.1</u> \pm 1.2
	Medium-Expert	97.9 \pm 1.6	95.9 \pm 6.0	92.7 \pm 2.8	98.9 \pm 8.5	101.1 \pm 5.2	<u>99.9</u> \pm 1.2
	Medium-Replay	45.8 \pm 0.2	49.0 \pm 0.4	42.1 \pm 3.6	48.1 \pm 0.2	51.0 \pm 0.8	<u>50.6</u> \pm 0.5
	Full-Replay	74.5 \pm 1.6	<u>79.5</u> \pm 1.5	75.0 \pm 0.7	76.7 \pm 2.3	82.1 \pm 1.1	79.3 \pm 0.9
Hopper	Random	8.6 \pm 0.2	20.1 \pm 11.6	<u>10.1</u> \pm 5.9	8.5 \pm 1.4	8.1 \pm 2.4	9.4 \pm 1.5
	Medium	62.0 \pm 3.0	78.3 \pm 4.4	65.2 \pm 4.2	81.8 \pm 9.8	102.0 \pm 1.0	<u>92.7</u> \pm 7.2
	Expert	108.2 \pm 4.2	83.9 \pm 6.0	<u>108.8</u> \pm 3.1	79.1 \pm 26.6	100.1 \pm 8.3	112.3 \pm 0.4
	Medium-Expert	103.3 \pm 9.2	<u>110.8</u> \pm 2.6	85.5 \pm 29.7	109.1 \pm 4.5	107.0 \pm 6.4	111.0 \pm 2.1
	Medium-Replay	47.4 \pm 35.4	98.9 \pm 2.0	89.6 \pm 13.2	<u>100.8</u> \pm 0.7	98.1 \pm 5.3	101.3 \pm 0.6
	Full-Replay	90.3 \pm 22.9	97.1 \pm 17.8	104.4 \pm 10.8	105.6 \pm 0.6	<u>107.1</u> \pm 0.4	107.2 \pm 0.5
Walker2d	Random	5.9 \pm 3.5	1.2 \pm 1.5	11.3 \pm 7.0	12.5 \pm 10.6	18.4 \pm 4.5	<u>15.6</u> \pm 6.4
	Medium	62.0 \pm 3.0	84.2 \pm 4.7	80.7 \pm 3.4	<u>89.6</u> \pm 0.3	82.5 \pm 3.6	92.4 \pm 5.4
	Expert	108.2 \pm 4.2	84.8 \pm 49.0	96.9 \pm 32.3	<u>111.5</u> \pm 0.1	112.3 \pm 0.2	110.8 \pm 0.1
	Medium-Expert	103.3 \pm 9.2	88.2 \pm 40.7	112.1 \pm 0.5	110.1 \pm 0.5	<u>111.6</u> \pm 0.3	111.1 \pm 0.3
	Medium-Replay	76.6 \pm 12.7	84.5 \pm 12.3	75.4 \pm 9.3	93.4 \pm 3.0	77.3 \pm 7.9	97.6 \pm 0.5
	Full-Replay	88.3 \pm 11.7	102.5 \pm 0.0	97.5 \pm 1.4	99.5 \pm 0.5	<u>102.2</u> \pm 1.7	102.1 \pm 0.2
MuJoCo Avg		70.7	74.2	72.9	77.8	<u>81.2</u>	<u>82.1</u>
Maze2d	Umaze	34.5 \pm 13.9	102.5 \pm 6.3	-8.9 \pm 6.1	73.1 \pm 13.8	<u>106.8</u> \pm 22.1	128.1 \pm 31.8
	Medium	63.3 \pm 63.3	90.4 \pm 29.6	34.8 \pm 2.7	87.4 \pm 48.7	<u>105.1</u> \pm 31.6	117.8 \pm 17.3
	Large	108.9 \pm 43.6	<u>177.7</u> \pm 34.2	61.7 \pm 3.5	123.3 \pm 70.5	78.3 \pm 61.7	195.8 \pm 31.3
Maze2d Avg		68.9	<u>123.53</u>	46.2	94.6	96.7	<u>147.2</u>
AntMaze	Umaze	100.0 \pm 0.0	92.5 \pm 8.3	83.3 \pm 4.5	97.5 \pm 5.0	<u>97.8</u> \pm 1.0	92.5 \pm 5.0
	Umaze-Diverse	87.5 \pm 12.5	32.5 \pm 34.9	70.6 \pm 3.7	75.0 \pm 20.8	<u>88.3</u> \pm 13.0	92.5 \pm 9.5
	Medium-Play	7.5 \pm 9.5	40.0 \pm 7.1	64.6 \pm 4.9	85.0 \pm 5.7	<u>84.0</u> \pm 4.2	85.0 \pm 12.9
	Medium-Diverse	12.5 \pm 12.5	40.0 \pm 25.5	61.7 \pm 6.1	85.0 \pm 12.9	<u>76.3</u> \pm 13.5	70.0 \pm 11.5
	Large-Play	2.5 \pm 5.0	5.0 \pm 8.7	42.5 \pm 6.5	65.0 \pm 19.1	<u>60.4</u> \pm 26.1	55.0 \pm 5.7
	Large-Diverse	2.5 \pm 5.0	22.5 \pm 14.8	27.6 \pm 7.8	65.0 \pm 10.0	<u>54.4</u> \pm 25.1	52.5 \pm 18.9
AntMaze Avg		35.4	38.75	58.3	<u>78.7</u>	<u>76.8</u>	<u>74.5</u>
Pen	Human	53.8 \pm 15.7	-2.1 \pm 0.0	<u>81.5</u> \pm 17.5	39.9 \pm 12.8	103.5 \pm 14.1	81.1 \pm 8.1
	Cloned	71.7 \pm 21.5	6.5 \pm 6.0	<u>77.2</u> \pm 17.7	34.6 \pm 11.3	91.8 \pm 21.7	<u>87.2</u> \pm 4.2
	Expert	126.6 \pm 24.8	51.5 \pm 38.4	133.6 \pm 16.0	<u>141.8</u> \pm 11.8	154.1 \pm 5.4	141.2 \pm 9.4
Door	Human	0.0 \pm 0.0	-0.2 \pm 0.0	3.1 \pm 2.0	-0.2 \pm 0.0	<u>0.0</u> \pm 0.0	0.0 \pm 0.0
	Cloned	0.0 \pm 0.0	-0.3 \pm 0.0	<u>0.8</u> \pm 1.0	0.0 \pm 0.0	1.1 \pm 2.6	0.0 \pm 0.0
	Expert	81.6 \pm 16.3	-0.3 \pm 0.0	<u>105.3</u> \pm 2.8	51.4 \pm 55.3	104.6 \pm 2.4	105.6 \pm 0.4
Hammer	Human	0.0 \pm 0.0	1.1 \pm 0.4	2.5 \pm 1.9	0.0 \pm 0.1	0.2 \pm 0.2	<u>2.2</u> \pm 3.2
	Cloned	0.1 \pm 0.0	0.3 \pm 0.0	1.1 \pm 0.5	0.1 \pm 0.1	<u>6.7</u> \pm 3.7	12.0 \pm 9.1
	Expert	<u>132.8</u> \pm 0.4	0.3 \pm 0.1	129.6 \pm 71.5	57.6 \pm 0.1	133.8 \pm 0.7	128.6 \pm 0.4
Relocate	Human	0.0 \pm 0.0	-0.3 \pm 0.0	<u>0.1</u> \pm 0.1	0.1 \pm 0.0	0.0 \pm 0.0	0.1 \pm 0.2
	Cloned	0.0 \pm 0.0	-0.3 \pm 0.0	<u>0.2</u> \pm 0.4	0.1 \pm 0.0	0.9 \pm 1.6	0.0 \pm 0.0
	Expert	90.6 \pm 18.2	-0.3 \pm 0.0	106.5 \pm 2.5	6.7 \pm 4.6	<u>106.6</u> \pm 3.2	111.2 \pm 2.4
Adroit Avg		46.4	4.65	<u>53.4</u>	28.8	<u>58.6</u>	<u>55.7</u>
Total Avg		57.7	51.2	62.6	64.2	<u>74.8</u>	<u>77.9</u>

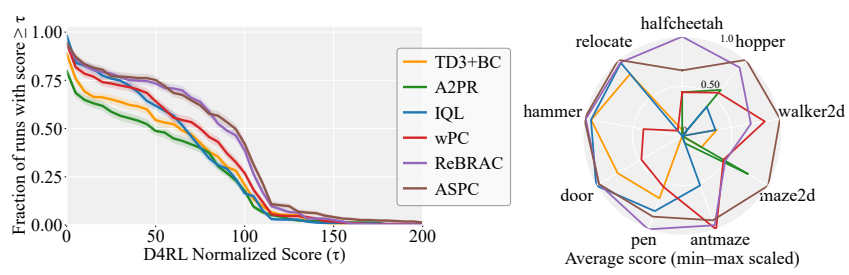


Figure 2: Left: performance profiles on 39 datasets of D4RL. Right: radar chart of the mean performance across the nine tasks.

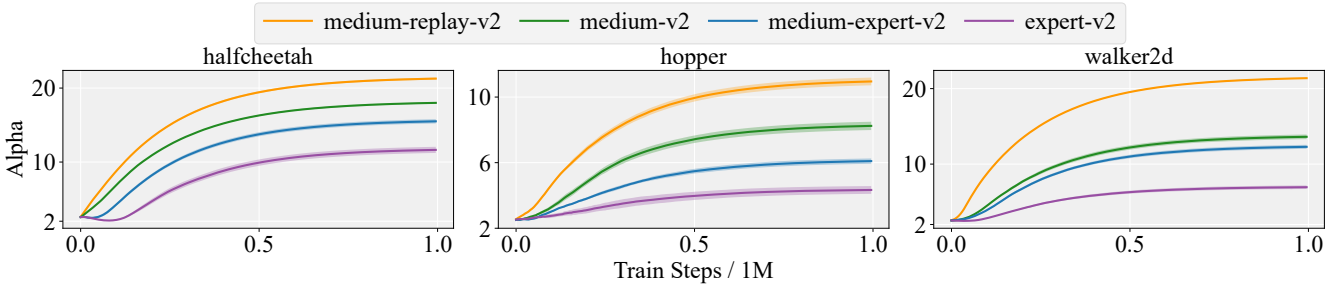


Figure 3: Learning curves of α on halfcheetah, hopper, and walker2d across datasets of different quality. Higher-quality datasets yield smaller α (favoring BC), while lower-quality ones yield larger α (favoring RL). α is initialized to 2.5.

5.2 Adaptability of the Scale Factor α

Dataset Adaptability Figure 3 shows the evolution of α on HalfCheetah, Hopper, and Walker2d for four dataset quality levels, listed from highest to lowest as expert, medium-expert, medium, and medium-replay. Across all three tasks, higher-quality datasets lead to smaller α , which places more weight on BC, whereas lower-quality datasets lead to larger α , shifting the emphasis toward RL. The consistent ordering confirms that ASPC automatically adjusts the policy-constraint scale to dataset quality without any per-dataset hyperparameter tuning.

Task Adaptability Figure 4 plots the α trajectories on six heterogeneous tasks. Tasks such as door, pen, hammer, and relocate possess narrow expert data distributions; here α settles near 10^{-1} , giving greater weight to BC. Conversely, antmaze and maze2d, whose datasets contain highly sub-optimal trajectories, drive α above 10, shifting emphasis to RL. This task-aware scaling requires no manual tuning and highlights ASPC’s cross-task adaptability.

Training Adaptability Combining the curves from Figures 4 and 3, we observe a common learning dynamic: α first drops (or rises only slightly) during the early training phase, indicating greater reliance on BC when the policy is still immature. As learning progresses and the critic stabilises, α gradually increases, handing more control to RL. This smooth, stage-wise adjustment underpins ASPC’s stable convergence across tasks and datasets.

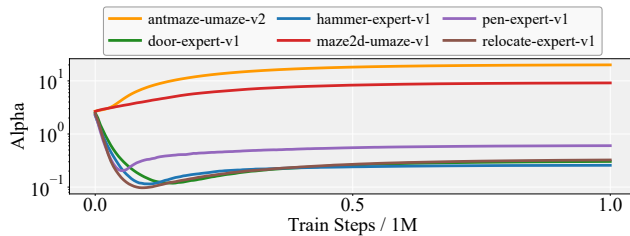


Figure 4: Learning curves of α on six different tasks. The algorithm automatically adjusts α based on the task characteristics. The y-axis uses logarithmic scaling to better visualize the differences of α across tasks. α is initialized to 2.5.

Table 2: Results under different α settings. % represents the percent difference from Navie.

Domain	Naive	Converged	Linear	Dynamic (ASPC)
Mujoco	70.3	79.3	77.0	82.1
Maze2d	61.9	133.2	103.3	147.2
AntMaze	28.7	64.1	56.3	74.5
Adroit	49.9	49.1	47.6	55.7
Total Avg	57.0	71.8 ↑25.9%	66.7 ↑17.0%	77.9 ↑36.6%

5.3 Necessity of Dynamic α Adjustment

As shown in Table 1, the hyperparameters meticulously selected via grid search ultimately underperform compared to the ASPC algorithm, which dynamically adjusts hyperparameters during training. This observation prompts the following question: is grid search simply missing the best setting, or is the dynamic adjustment performed by ASPC the real source of its advantage? To answer this, we conduct three controlled tests.

- **Naive α .** TD3+BC is run with a fixed scale factor $\alpha = 2.5$.
- **Converged α .** TD3+BC is run with α fixed to the final value reached by ASPC on the same dataset.
- **Linear α .** TD3+BC starts from $\alpha = 2.5$ and linearly interpolates to the above converged value over the training horizon.

To ensure fairness, all TD3+BC variants employ the same robust critic architecture as ASPC: three hidden layers, each followed by a LayerNorm.

Table 2 summarises the mean normalised scores in the four D4RL domains. Percentages in blue report the relative gain over the naive baseline that fixes $\alpha = 2.5$. Converged α and Linear α both outperform the naive setting, which confirms that the value to which ASPC eventually converges is a much more appropriate scale for the policy constraint. ASPC (Dynamic α) still exceeds the Converged variant by a wide margin, and the Linear schedule closes only part of the gap. These results show that simply finding a good fixed α is not enough. Adapting the scale throughout training is essential for the best performance. ASPC provides this

dynamic adjustment automatically and therefore achieves the highest overall score.

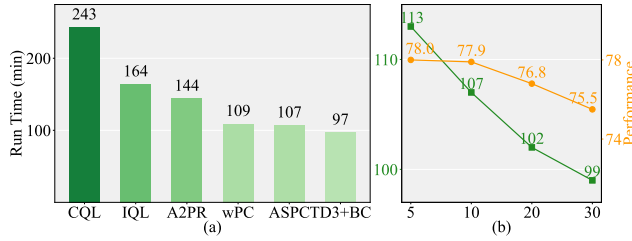


Figure 5: (a) Runtime comparison of different algorithms. (b) Runtime and average performance under different α -update intervals (k_α). ASPC introduces only minimal overhead compared to TD3+BC, and increasing the update interval reduces runtime while maintaining high performance.

5.4 Runtime Analysis

ASPC employs second-order gradient computations for updating α , which increases cost. However, its update interval (k_α) can be set substantially longer than that of the actor (k_π), thereby minimizing the additional computational overhead. To evaluate runtime efficiency, we compare the execution time of one million iterations of ASPC against that of other baseline algorithms. Figure 5 presents a bar chart comparing the runtime of ASPC against TD3+BC, CQL, IQL, wPC and A2PR on the halfcheetah-medium-v2 dataset. The results indicate that ASPC introduces only a minimal additional computational overhead beyond that of TD3+BC.

We further analyze the relationship between k_α , runtime, and performance, as illustrated in Figure 5. The baseline setting for k_α is 10, with an α learning rate of 2×10^{-3} . By scaling the learning rate of α proportionally to k_α , we observe that reducing k_α does not lead to significant performance degradation. This suggests that ASPC effectively captures the correct gradient optimization direction, maintaining robustness even when the gradient step size is large. When k_α is set to 30, the runtime is nearly identical to that of TD3+BC while maintaining strong performance. This highlights the efficiency of the ASPC algorithm.

5.5 Ablation Studies

Robust Critic(RC) When using the original TD3+BC critic network (with two hidden layers and no LayerNorm), during the process of adjusting α , Q-values exhibit significant instability, frequently leading to overestimation, causing catastrophic failure of the algorithm. Since wPC is also designed based on the original TD3+BC framework, we include it in our experiments related to RC (with three hidden layers and LayerNorm). Figure 6 presents the experimental results. The results indicate that when RC is not utilized, both wPC and ASPC achieve limited performance improvement and even exhibit performance degradation on certain tasks.

Loss Function Figure 7 reveals clear, domain-dependent effects when the regularization terms are added to the base

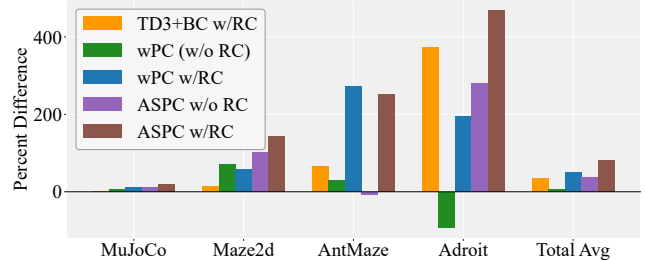


Figure 6: Percent difference relative to the baseline TD3+BC (critic with three hidden layers, each incorporating LayerNorm).

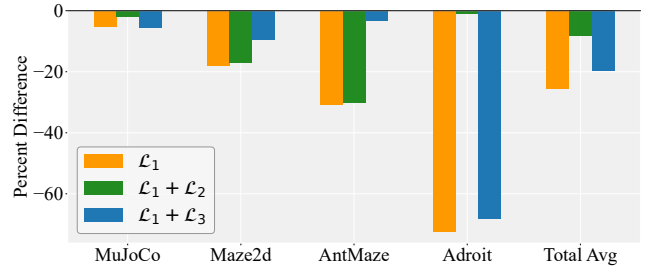


Figure 7: Percent difference of outer loss variants (10) relative to the full ASPC configuration.

loss \mathcal{L}_1 . Adding neither term (\mathcal{L}_1 only) gives the poorest performance. Introducing only \mathcal{L}_2 lifts performance in MuJoCo and Adroit to the level of full ASPC, while leaving AntMaze almost unchanged. Conversely, adding only \mathcal{L}_3 significantly boosts AntMaze but has little effect on MuJoCo or Adroit. For Maze2D, neither single term suffices. Only the full loss $\mathcal{L}_1 + \mathcal{L}_2 + \mathcal{L}_3$ attains the best result. These results can be explained by Proposition 4.3, which shows that \mathcal{L}_2 and \mathcal{L}_3 implicitly constrain one another. Consequently, adding \mathcal{L}_2 in MuJoCo and Adroit implicitly bounds ΔL_{BC} as well, so the single-step performance guarantee of Theorem 4.5 is already satisfied. Conversely, in AntMaze a direct \mathcal{L}_3 penalty implicitly limits $(\Delta Q)^2$, again meeting the theorem’s lower bound. For Maze2D, however, neither implicit relation is strong enough; both \mathcal{L}_2 and \mathcal{L}_3 must be enforced explicitly for the condition in Theorem 4.5 to hold.

6 Conclusion

We presented Adaptive Scaling of Policy Constraints (ASPC), a bi-level framework that adjusts the RL-BC trade-off by optimizing the scaling factor α through second-order updates. We also provide a theoretical performance improvement guarantee. A single hyperparameter setting suffices for all D4RL domains we evaluated, and the additional computational overhead is negligible. These results demonstrate that dynamic hyperparameter tuning can substantially improve the adaptability of offline RL. Future work includes integrating ASPC with other offline algorithms and assessing its effectiveness on real-world data and larger benchmark suites.

References

An, G.; Moon, S.; Kim, J.-H.; and Song, H. O. 2021. Uncertainty-based offline reinforcement learning with diversified q-ensemble. *Advances in neural information processing systems*, 34: 7436–7447.

Bai, C.; Wang, L.; Yang, Z.; Deng, Z.; Garg, A.; Liu, P.; and Wang, Z. 2022. Pessimistic bootstrapping for uncertainty-driven offline reinforcement learning. *arXiv preprint arXiv:2202.11566*.

Ball, P. J.; Smith, L.; Kostrikov, I.; and Levine, S. 2023. Efficient online reinforcement learning with offline data. In *International Conference on Machine Learning*, 1577–1594. PMLR.

Chen, L.; Lu, K.; Rajeswaran, A.; Lee, K.; Grover, A.; Laskin, M.; Abbeel, P.; Srinivas, A.; and Mordatch, I. 2021. Decision transformer: Reinforcement learning via sequence modeling. *Advances in neural information processing systems*, 34: 15084–15097.

Chen, X.-H.; Luo, F.-M.; Yu, Y.; Li, Q.; Qin, Z.; Shang, W.; and Ye, J. 2023. Offline model-based adaptable policy learning for decision-making in out-of-support regions. *IEEE Transactions on Pattern Analysis and Machine Intelligence*, 45(12): 15260–15274.

El Sallab, A.; Abdou, M.; Perot, E.; and Yogamani, S. 2017. Deep Reinforcement Learning framework for Autonomous Driving. *stat*, 1050: 8.

Finn, C.; Abbeel, P.; and Levine, S. 2017. Model-agnostic meta-learning for fast adaptation of deep networks. In *International conference on machine learning*, 1126–1135. PMLR.

Franceschi, L.; Frasconi, P.; Salzo, S.; Grazzi, R.; and Pontil, M. 2018. Bilevel programming for hyperparameter optimization and meta-learning. In *International conference on machine learning*, 1568–1577. PMLR.

Fujimoto, S.; and Gu, S. S. 2021. A minimalist approach to offline reinforcement learning. *Advances in neural information processing systems*, 34: 20132–20145.

Fujimoto, S.; Meger, D.; and Precup, D. 2019. Off-policy deep reinforcement learning without exploration. In *International conference on machine learning*, 2052–2062. PMLR.

Hong, Z.-W.; Agrawal, P.; Combes, R. T. d.; and Laroche, R. 2023. Harnessing mixed offline reinforcement learning datasets via trajectory weighting. *arXiv preprint arXiv:2306.13085*.

Janner, M.; Li, Q.; and Levine, S. 2021. Offline reinforcement learning as one big sequence modeling problem. *Advances in neural information processing systems*, 34: 1273–1286.

Kakade, S.; and Langford, J. 2002. Approximately optimal approximate reinforcement learning. In *Proceedings of the nineteenth international conference on machine learning*, 267–274.

Kendall, A.; Hawke, J.; Janz, D.; Mazur, P.; Reda, D.; Allen, J.-M.; Lam, V.-D.; Bewley, A.; and Shah, A. 2019. Learning to drive in a day. In *2019 international conference on robotics and automation (ICRA)*, 8248–8254. IEEE.

Kidambi, R.; Rajeswaran, A.; Netrapalli, P.; and Joachims, T. 2020. Morel: Model-based offline reinforcement learning. *Advances in neural information processing systems*, 33: 21810–21823.

Kingma, D. P. 2014. Adam: A method for stochastic optimization. *arXiv preprint arXiv:1412.6980*.

Kostrikov, I.; Nair, A.; and Levine, S. 2022. Offline Reinforcement Learning with Implicit Q-Learning. In *International Conference on Learning Representations*.

Kumar, A.; Agarwal, R.; Geng, X.; Tucker, G.; and Levine, S. 2022. Offline q-learning on diverse multi-task data both scales and generalizes. *arXiv preprint arXiv:2211.15144*.

Kumar, A.; Zhou, A.; Tucker, G.; and Levine, S. 2020. Conservative q-learning for offline reinforcement learning. *Advances in Neural Information Processing Systems*, 33: 1179–1191.

Lee, K.-H.; Nachum, O.; Yang, M. S.; Lee, L.; Freeman, D.; Guadarrama, S.; Fischer, I.; Xu, W.; Jang, E.; Michalewski, H.; et al. 2022. Multi-game decision transformers. *Advances in Neural Information Processing Systems*, 35: 27921–27936.

Levine, S.; Kumar, A.; Tucker, G.; and Fu, J. 2020. Offline reinforcement learning: Tutorial, review, and perspectives on open problems. *arXiv preprint arXiv:2005.01643*.

Liu, T.; Li, Y.; Lan, Y.; Gao, H.; Pan, W.; and Xu, X. 2024. Adaptive Advantage-Guided Policy Regularization for Offline Reinforcement Learning. In *International Conference on Machine Learning*, 31406–31424. PMLR.

Liu, Y.; and Hofert, M. 2024. Implicit and Explicit Policy Constraints for Offline Reinforcement Learning. In *Causal Learning and Reasoning*, 499–513. PMLR.

Nikulin, A.; Kurenkov, V.; Tarasov, D.; and Kolesnikov, S. 2023. Anti-exploration by random network distillation. In *International Conference on Machine Learning*, 26228–26244. PMLR.

Peng, Z.; Han, C.; Liu, Y.; and Zhou, Z. 2023. Weighted policy constraints for offline reinforcement learning. In *Proceedings of the AAAI Conference on Artificial Intelligence*, volume 37, 9435–9443.

Prasad, N.; Cheng, L. F.; Chivers, C.; Draugelis, M.; and Engelhardt, B. E. 2017. A reinforcement learning approach to weaning of mechanical ventilation in intensive care units. In *33rd Conference on Uncertainty in Artificial Intelligence, UAI 2017*.

Ran, Y.; Li, Y.-C.; Zhang, F.; Zhang, Z.; and Yu, Y. 2023. Policy regularization with dataset constraint for offline reinforcement learning. In *International Conference on Machine Learning*, 28701–28717. PMLR.

Ren*, J.; Feng*, X.; Liu*, B.; Pan*, X.; Fu, Y.; Mai, L.; and Yang, Y. 2023. TorchOpt: An Efficient Library for Differentiable Optimization. *Journal of Machine Learning Research*, 24(367): 1–14.

Tarasov, D.; Kurenkov, V.; Nikulin, A.; and Kolesnikov, S. 2024a. Revisiting the minimalist approach to offline reinforcement learning. *Advances in Neural Information Processing Systems*, 36.

Tarasov, D.; Nikulin, A.; Akimov, D.; Kurenkov, V.; and Kolesnikov, S. 2024b. CORL: Research-oriented deep offline reinforcement learning library. *Advances in Neural Information Processing Systems*, 36.

Wang, L.; Zhang, W.; He, X.; and Zha, H. 2018. Supervised reinforcement learning with recurrent neural network for dynamic treatment recommendation. In *Proceedings of the 24th ACM SIGKDD international conference on knowledge discovery & data mining*, 2447–2456.

Xiong, H.; Xu, T.; Zhao, L.; Liang, Y.; and Zhang, W. 2022. Deterministic policy gradient: Convergence analysis. In *Uncertainty in Artificial Intelligence*, 2159–2169. PMLR.

Yang, Q.; Wang, S.; Lin, M. G.; Song, S.; and Huang, G. 2023. Boosting offline reinforcement learning with action preference query. In *International Conference on Machine Learning*, 39509–39523. PMLR.

Yang, Q.; Wang, S.; Zhang, Q.; Huang, G.; and Song, S. 2024. Hundreds Guide Millions: Adaptive Offline Reinforcement Learning With Expert Guidance. *IEEE transactions on neural networks and learning systems*, 35(11): 16288–16300.

Yu, T.; Kumar, A.; Rafailov, R.; Rajeswaran, A.; Levine, S.; and Finn, C. 2021. Combo: Conservative offline model-based policy optimization. *Advances in neural information processing systems*, 34: 28954–28967.

Yu, T.; Thomas, G.; Yu, L.; Ermon, S.; Zou, J. Y.; Levine, S.; Finn, C.; and Ma, T. 2020. Mopo: Model-based offline policy optimization. *Advances in Neural Information Processing Systems*, 33: 14129–14142.

Yuan, Z.; Zhang, Z.; Li, X.; Cui, Y.; Li, M.; and Ban, X. 2024. Controlling partially observed industrial system based on offline reinforcement learning—A case study of paste thickener. *IEEE Transactions on Industrial Informatics*.

Zhan, X.; Xu, H.; Zhang, Y.; Zhu, X.; Yin, H.; and Zheng, Y. 2022. Deepthermal: Combustion optimization for thermal power generating units using offline reinforcement learning. In *Proceedings of the AAAI Conference on Artificial Intelligence*, volume 36, 4680–4688.

Zhang, J.; Lyu, J.; Ma, X.; Yan, J.; Yang, J.; Wan, L.; and Li, X. 2023. Uncertainty-driven trajectory truncation for data augmentation in offline reinforcement learning. In *ECAI 2023*, 3018–3025. IOS Press.

A Theoretical Proofs

A.1 Proof of Proposition 4.3

Throughout the argument, we write:

$$\begin{aligned}\Delta L_{BC} &:= |L_{t+1}^{BC} - L_t^{BC}|, \\ x &:= \mathbb{E}_s \|\pi_{t+1}(s) - \pi_t(s)\|^2, \\ c &:= \sqrt{L_t^{BC}}.\end{aligned}$$

Lemma A.1 (Reverse triangle inequality). *For all $A, B \in \mathbb{R}$ one has $|A + B| \geq ||A| - |B||$.*

Lemma A.2 (Cauchy–Schwarz). *For square-integrable real random variables X, Y , $|\mathbb{E}[XY]| \leq (\mathbb{E}[X^2])^{1/2} (\mathbb{E}[Y^2])^{1/2}$.*

Proof. The proof proceeds in three steps.

Step 1: A lower bound on ΔL_{BC} . Expand the definition of ΔL_{BC} and simplify:

$$\begin{aligned}\Delta L_{BC} &= \left| \mathbb{E}_s \left[\|\pi_{t+1}(s) - \pi_\beta(s)\|^2 - \|\pi_t(s) - \pi_\beta(s)\|^2 \right] \right| \\ &= \left| \mathbb{E}_s \left[(\pi_{t+1}(s) - \pi_\beta(s))^\top (\pi_{t+1}(s) - \pi_\beta(s)) \right. \right. \\ &\quad \left. \left. - (\pi_t(s) - \pi_\beta(s))^\top (\pi_t(s) - \pi_\beta(s)) \right] \right| \\ &= \left| \mathbb{E}_s \left[(\pi_{t+1}(s) - \pi_\beta(s) + \pi_t(s) - \pi_\beta(s))^\top \right. \right. \\ &\quad \left. \left. (\pi_{t+1}(s) - \pi_t(s)) \right] \right| \\ &= \left| \mathbb{E}_s \left[\|\pi_{t+1}(s) - \pi_t(s)\|^2 \right. \right. \\ &\quad \left. \left. + 2(\pi_t(s) - \pi_\beta(s))^\top (\pi_{t+1}(s) - \pi_t(s)) \right] \right| \\ &= \left| x + 2 \mathbb{E}_s \left[(\pi_t(s) - \pi_\beta(s))^\top (\pi_{t+1}(s) - \pi_t(s)) \right] \right| \\ &\stackrel{A.1}{\geq} \left| |x| - 2 \left| \mathbb{E}_s \left[(\pi_t(s) - \pi_\beta(s))^\top (\pi_{t+1}(s) - \pi_t(s)) \right] \right| \right| \\ &\stackrel{A.2}{\geq} \left| x - 2 \sqrt{\mathbb{E}_s \|\pi_t(s) - \pi_\beta(s)\|^2} \right. \\ &\quad \left. - \sqrt{\mathbb{E}_s \|\pi_{t+1}(s) - \pi_t(s)\|^2} \right| \\ &= \left| x - 2c\sqrt{x} \right|\end{aligned}\tag{19}$$

Consequently

$$\Delta L_{BC} \geq |x - 2c\sqrt{x}| = \begin{cases} 2c\sqrt{x} - x, & 0 \leq x < 4c^2, \\ x - 2c\sqrt{x}, & x \geq 4c^2. \end{cases}\tag{20}$$

Step 2: An upper bound on $(\Delta Q)^2$. Jensen's inequality and

the assumption 4.2 yield

$$\begin{aligned}(\Delta Q)^2 &= \left(\mathbb{E}_s [Q(s, \pi_{t+1}(s)) - Q(s, \pi_t(s))] \right)^2 \\ &\leq \mathbb{E}_s [(Q(s, \pi_{t+1}(s)) - Q(s, \pi_t(s)))^2] \\ &\leq L_Q^2 \mathbb{E}_s \|\pi_{t+1}(s) - \pi_t(s)\|^2 \\ &= L_Q^2 x\end{aligned}\tag{21}$$

Step 3: Mutual bounds. According to (21),

$$x \geq \frac{(\Delta Q)^2}{L_Q^2} =: x_{\min}.$$

From (20) we note that $f(x) = 2c\sqrt{x} - x$ is increasing on $[0, c^2]$ and decreasing on $[c^2, 4c^2]$, whereas $g(x) = x - 2c\sqrt{x}$ is increasing on $[4c^2, \infty)$. Hence, substituting x_{\min} (or the end-point $4c^2$ in the middle band) yields a valid lower bound in each interval of x :

$$\Delta L_{BC} \geq \begin{cases} 2c \frac{|\Delta Q|}{L_Q} - \frac{(\Delta Q)^2}{L_Q^2}, & 0 \leq x \leq c^2, \\ 0, & c^2 \leq x \leq 4c^2, \\ \frac{(\Delta Q)^2}{L_Q^2} - 2c \frac{|\Delta Q|}{L_Q}, & x \geq 4c^2. \end{cases}\tag{22}$$

Equivalently,

$$\Delta L_{BC} \geq \max \left\{ 2c \frac{|\Delta Q|}{L_Q} - \frac{(\Delta Q)^2}{L_Q^2}, 0, \right. \tag{23}$$

$$\left. \frac{(\Delta Q)^2}{L_Q^2} - 2c \frac{|\Delta Q|}{L_Q} \right\}.\tag{24}$$

Similarly, using (20) we obtain the following upper bounds for x :

$$x \leq (c + \sqrt{c^2 + \Delta L_{BC}})^2.\tag{25}$$

Combining (21) with (25) gives an upper bound on $(\Delta Q)^2$:

$$(\Delta Q)^2 \leq L_Q^2 (c + \sqrt{c^2 + \Delta L_{BC}})^2.\tag{26}$$

Equations (23) and (26) together yield the desired mutual bounds. \square

A.2 Proof of Proposition 4.4

This section analyses conditions under which the one-step performance difference $J(\pi_{t+1}) - J(\pi_t)$ admits a tractable lower bound when training on a fixed offline dataset D collected under behavior policy π_β (so $D \approx d_{\pi_\beta}$).

Lemma A.3 (Performance-difference lemma). *For any policies π_1 and π_2 ,*

$$\begin{aligned}J(\pi_1) - J(\pi_2) &= \frac{1}{1-\gamma} \mathbb{E}_{s \sim d_{\pi_1}} [\mathbb{E}_{a \sim \pi_1} Q^{\pi_2}(s, a) - V^{\pi_2}(s)].\end{aligned}\tag{27}$$

The proof of Lemma A.3 can be found in (Kakade and Langford 2002).

Lemma A.4. *Under Assumption 4.2, the total variation distance between the visitation distributions of any policy π and the behavior policy π_β satisfies*

$$\begin{aligned} \|d_\pi - d_{\pi_\beta}\|_1 &= \int_s |d_\pi(s) - d_{\pi_\beta}(s)| \, ds \\ &\leq C L_P \max_{s \in \mathcal{S}} \|\pi(s) - \pi_\beta(s)\|. \end{aligned} \quad (28)$$

where $C > 0$ is a constant.

The proof of Lemma A.4 can be found in the appendix of (Xiong et al. 2022).

Lemma A.5 (Sup-norm version of (25)). *Define*

$$\begin{aligned} x_\infty &:= \sup_s \|\pi_{t+1}(s) - \pi_t(s)\|^2, \\ c_\infty^2 &:= \sup_s \|\pi_t(s) - \pi_\beta(s)\|^2, \\ \Delta L_\infty^{BC} &:= \sup_s |\|\pi_{t+1}(s) - \pi_\beta(s)\|^2 - \|\pi_t(s) - \pi_\beta(s)\|^2|. \end{aligned}$$

Then

$$x_\infty \leq (c_\infty + \sqrt{c_\infty^2 + \Delta L_\infty^{BC}})^2. \quad (29)$$

Proof. For each s , let $\Delta L_{BC}(s) = \|\pi_{t+1}(s) - \pi_\beta(s)\|^2 - \|\pi_t(s) - \pi_\beta(s)\|^2$. Then

$$\begin{aligned} \|\pi_{t+1}(s) - \pi_t(s)\|^2 &= [(\pi_{t+1}(s) - \pi_\beta(s)) - (\pi_t(s) - \pi_\beta(s))]^2 \\ &\leq (\|\pi_{t+1}(s) - \pi_\beta(s)\| + \|\pi_t(s) - \pi_\beta(s)\|)^2 \\ &= \left(\sqrt{\|\pi_{t+1}(s) - \pi_\beta(s)\|^2 + \|\pi_t(s) - \pi_\beta(s)\|^2} \right)^2 \\ &= \left(\sqrt{\|\pi_t(s) - \pi_\beta(s)\|^2 + \Delta L_{BC}(s)} + \|\pi_t(s) - \pi_\beta(s)\| \right)^2 \\ &\leq (c_\infty + \sqrt{c_\infty^2 + \Delta L_\infty^{BC}})^2. \end{aligned} \quad (30)$$

Taking the supremum over s gives the stated result:

$$\begin{aligned} x_\infty &= \sup_s \|\pi_{t+1}(s) - \pi_t(s)\|^2 \\ &\leq (c_\infty + \sqrt{c_\infty^2 + \Delta L_\infty^{BC}})^2. \end{aligned} \quad (31)$$

The proof of Lemma A.5 is finished. \square

Proof. In our deterministic setting, the conditional action distribution $\pi(\cdot|s)$ for any state s is a Dirac measure concentrated at a single action. Specifically, for π_2 in Lemma A.3 we have:

$$V^{\pi_2}(s) = \mathbb{E}_{a \sim \pi_2}[Q^{\pi_2}(s, a)] = Q^{\pi_2}(s, \pi_2(s)), \quad (32)$$

Applying Lemma A.3 with $\pi_1 = \pi_{t+1}$ and $\pi_2 = \pi_t$ gives:

$$\begin{aligned} J(\pi_{t+1}) - J(\pi_t) &= \frac{1}{1-\gamma} \mathbb{E}_{s \sim d_{\pi_{t+1}}} [Q^{\pi_t}(s, \pi_{t+1}(s)) - Q^{\pi_t}(s, \pi_t(s))]. \end{aligned} \quad (33)$$

Write the performance-difference identity (33) as

$$\begin{aligned} J(\pi_{t+1}) - J(\pi_t) &= \frac{1}{1-\gamma} \mathbb{E}_{s \sim d_{\pi_{t+1}}} [Q^{\pi_t}(s, \pi_{t+1}(s)) - Q^{\pi_t}(s, \pi_t(s))] \\ &= \frac{1}{1-\gamma} \left\{ \mathbb{E}_{s \sim D} [Q^{\pi_t}(s, \pi_{t+1}(s)) - Q^{\pi_t}(s, \pi_t(s))] \right. \\ &\quad \left. + \int (d_{\pi_{t+1}}(s) - D(s)) (Q^{\pi_t}(s, \pi_{t+1}(s)) - Q^{\pi_t}(s, \pi_t(s))) \, ds \right\} \\ &\geq \frac{1}{1-\gamma} \left\{ \underbrace{\mathbb{E}_{s \sim D} [Q^{\pi_t}(s, \pi_{t+1}(s)) - Q^{\pi_t}(s, \pi_t(s))]}_{\Delta Q} \right. \\ &\quad \left. - \left| \int (d_{\pi_{t+1}}(s) - D(s)) (Q^{\pi_t}(s, \pi_{t+1}(s)) - Q^{\pi_t}(s, \pi_t(s))) \, ds \right| \right\} \\ &\geq \frac{1}{1-\gamma} \left\{ \Delta Q - \|d_{\pi_{t+1}} - d_{\pi_\beta}\|_1 \cdot \right. \\ &\quad \left. \sup_s |Q^{\pi_t}(s, \pi_{t+1}(s)) - Q^{\pi_t}(s, \pi_t(s))| \right\} \\ &\stackrel{A.4}{\geq} \frac{1}{1-\gamma} \left\{ \Delta Q - C L_P \max_s \|\pi_{t+1} - \pi_\beta\| \cdot \right. \\ &\quad \left. \sup_s |Q^{\pi_t}(s, \pi_{t+1}(s)) - Q^{\pi_t}(s, \pi_t(s))| \right\} \\ &\stackrel{A.2}{\geq} \frac{1}{1-\gamma} \left\{ \Delta Q - C L_P L_Q \max_s \|\pi_{t+1} - \pi_\beta\| \cdot \right. \\ &\quad \left. \max_s \|\pi_{t+1} - \pi_t\| \right\} \\ &\geq \frac{1}{1-\gamma} \left\{ \Delta Q - C L_P L_Q (\max_s \|\pi_{t+1} - \pi_t\| + \right. \\ &\quad \left. \max_s \|\pi_t - \pi_\beta\|) \max_s \|\pi_{t+1} - \pi_t\| \right\} \\ &= \frac{1}{1-\gamma} \left\{ \Delta Q - C L_P L_Q (\sqrt{x_\infty} + c_\infty) \sqrt{x_\infty} \right\} \\ &\stackrel{A.5}{\geq} \frac{1}{1-\gamma} \left\{ \Delta Q - C L_P L_Q \left[(c_\infty + \sqrt{c_\infty^2 + \Delta L_\infty^{BC}})^2 \right. \right. \\ &\quad \left. \left. + c_\infty \sqrt{c_\infty^2 + \Delta L_\infty^{BC} + c_\infty^2} \right] \right\} \\ &= \frac{1}{1-\gamma} \left\{ \Delta Q - C L_P L_Q (3c_\infty^2 + 3c_\infty \sqrt{c_\infty^2 + \Delta L_\infty^{BC}} + \right. \\ &\quad \left. \Delta L_\infty^{BC}) \right\}. \end{aligned} \quad (34)$$

Thus, the one-step performance satisfies the lower bound

$$\begin{aligned} J(\pi_{t+1}) - J(\pi_t) &\geq \frac{1}{1-\gamma} \left(\Delta Q - \kappa (3c_\infty^2 + 3c_\infty \sqrt{c_\infty^2 + \Delta L_\infty^{BC}} + \Delta L_\infty^{BC}) \right), \\ \kappa &:= C L_P L_Q. \end{aligned} \quad (35)$$

The proof of Proposition 4.4 is finished. \square

A.3 Proof of Theorem 4.5

We now show how our outer-loss components ensure the performance lower bound (35) is maintained.

\mathcal{L}_1 (7) updates α based on the relative gradients of Q-value and the BC loss. Under the initialization assumption $\nabla_\theta \mathbb{E}[Q] > \nabla_\theta L_{BC}$, so \mathcal{L}_1 updates α to favor Q-improvement.

In our algorithm, the two regularizers \mathcal{L}_2 and \mathcal{L}_3 play complementary roles in guaranteeing safe single-step improvements. Specifically, \mathcal{L}_2 in (8) penalizes the squared change in the Q-function, ΔQ^2 , to prevent overly large and unreliable Q-updates. In order to preserve the one-step performance lower bound (35), \mathcal{L}_3 in (9) must impose a matching penalty on the bias term identified in that bound. By choosing \mathcal{L}_3 so that its curvature mirrors that of \mathcal{L}_2 , we ensure the single-step performance guarantee remains non-negative.

Proof. We perform a second-order Taylor expansion of $\sqrt{c_\infty^2 + \Delta L_\infty^{BC}}$ around $\Delta L_\infty^{BC} = 0$, assuming $\Delta L_\infty^{BC}/c_\infty^2 \ll 1$, discarding higher-order and constant terms. Substituting into the square and retaining only terms up to $O(\Delta L_\infty^{BC})$ yields:

$$\begin{aligned}
\mathcal{L}_3 &= \kappa^2 \left(3c_\infty^2 + 3c_\infty \sqrt{c_\infty^2 + \Delta L_\infty^{BC}} + \Delta L_\infty^{BC} \right)^2 \\
&= \kappa^2 \left(3c_\infty^2 + 3c_\infty \left(c_\infty + \frac{\Delta L_\infty^{BC}}{2c_\infty} - \frac{(\Delta L_\infty^{BC})^2}{8c_\infty^3} \right) + O(\Delta L_\infty^{BC^3}) \right) + \Delta L_\infty^{BC} \\
&= \kappa^2 \left(6c_\infty^2 + \frac{5}{2} \Delta L_\infty^{BC} - \frac{3}{8} \frac{(\Delta L_\infty^{BC})^2}{c_\infty^2} + O(\Delta L_\infty^{BC^3}) \right)^2 \\
&= \kappa^2 \left(36c_\infty^4 + 30c_\infty^2 \Delta L_\infty^{BC} + O(\Delta L_\infty^{BC^2}) \right) \\
&= 36\kappa^2 c_\infty^4 + 30\kappa^2 c_\infty^2 \Delta L_\infty^{BC} + O(\Delta L_\infty^{BC^2}) \\
&\approx 30\kappa^2 c_\infty^2 \Delta L_\infty^{BC} \\
&= wc_\infty^2 \Delta L_\infty^{BC}, \quad w := 30k^2.
\end{aligned} \tag{36}$$

In practice, we scale \mathcal{L}_3 by the value of \mathcal{L}_2 to match its regularization strength and simply set w to 1:

$$\mathcal{L}_3 = (\Delta Q)^2 c_\infty^2 \Delta L_\infty^{BC}. \tag{37}$$

By setting an appropriate w , the algorithm can guarantee that:

$$J(\pi_{t+1}) - J(\pi_t) \geq 0. \tag{38}$$

The proof of Theorem 4.5 is finished. \square

A.4 Proof of Theorem 4.6

Proof. We split the total performance gap into two components:

$$\begin{aligned}
&J(\pi^*) - J(\pi_T) \\
&= [J(\pi^*) - J(\pi_0)] - [J(\pi_1) - J(\pi_0)] - \\
&\quad [J(\pi_2) - J(\pi_1)] - \cdots - [J(\pi_T) - J(\pi_{T-1})] \\
&= J(\pi^*) - J(\pi_0) - \sum_{i=0}^{T-1} [J(\pi_{i+1}) - J(\pi_i)].
\end{aligned} \tag{39}$$

We first observe that the behavior-cloning loss

$$L_t^{BC} = \mathbb{E}_{(s,a) \sim D} \|\pi_t(s) - a\|^2 \tag{40}$$

decreases rapidly during early training. Hence there exists a warm-up time t_0 such that

$$L_{t_0}^{BC} \leq \varepsilon_0 \implies \mathbb{E}_{s \sim D} \|\pi_{t_0}(s) - \beta(s)\| \leq \sqrt{\varepsilon_0}, \tag{41}$$

and we set

$$\pi_0 := \pi_{t_0} \approx \beta.$$

then

$$\begin{aligned}
&J(\pi^*) - J(\pi_0) \\
&= \frac{1}{1-\gamma} \left(\mathbb{E}_{s \sim d_{\pi^*}} [r(s)] - \mathbb{E}_{s \sim d_{\pi_0}} [r(s)] \right) \\
&= \frac{1}{1-\gamma} \int_s (d_{\pi^*}(s) - d_{\pi_0}(s)) r(s) \, ds \\
&\leq \frac{1}{1-\gamma} \int_s |d_{\pi^*}(s) - d_{\pi_0}(s)| R_{\max} \, ds \\
&= \frac{R_{\max}}{1-\gamma} \|d_{\pi^*} - d_{\pi_0}\|_1 \\
&\stackrel{A.4}{\leq} \frac{R_{\max}}{1-\gamma} C L_P \max_s \|\pi^*(s) - \pi_0(s)\| \\
&\leq \frac{C L_P R_{\max}}{1-\gamma} \left(\underbrace{\max_s \|\pi^*(s) - \beta(s)\|}_{\varepsilon_\beta} + \mathbb{E}_{s \sim D} \|\pi_0(s) - \beta(s)\| \right) \\
&\leq \frac{C L_P R_{\max}}{1-\gamma} (\varepsilon_\beta + \sqrt{\varepsilon_0}).
\end{aligned} \tag{42}$$

We define

$$\Delta_0 = \frac{C L_P R_{\max}}{1-\gamma} (\varepsilon_\beta + \sqrt{\varepsilon_0}) \tag{43}$$

Next, each one-step update i produces the gain (38)

$$\delta_i = J(\pi_{i+1}) - J(\pi_i) \geq 0. \tag{44}$$

Summing these gains yields the unified bound

$$J(\pi^*) - J(\pi_T) \leq \Delta_0 - \sum_{i=0}^{T-1} \delta_i. \tag{45}$$

With a fixed regularization weight α , the sequence $\{\delta_i\}$ tends to decay rapidly toward zero or even become negative. Therefore, static α leaves a large residual gap in (45). Our meta-update dynamically adjusts α so that each δ_i stays bounded below by a positive constant $\delta_{\min} > 0$ over a long horizon. Thus

$$J(\pi^*) - J(\pi_T) \leq \Delta_0 - T \delta_{\min}. \tag{46}$$

The proof of Theorem 4.6 is finished. \square

B Experimental Details

B.1 Hardware and Software

We use the following hardware: 1) Intel (R) Xeon (R) Platinum 8352V CPU @ 2.10 GHz; 2) NVIDIA GeForce RTX 4090 GPU. We use the following software versions: 1) Python 3.8.10; 2) D4RL 1.1; 3) MuJoCo 3.2.3; 4) Gym 0.23.1; 5) mujoco-py 2.1.2.14; 6) PyTorch 2.2.2 + CUDA 12.1; 7) TorchOpt 0.7.3.

B.2 Hyperparameters

The network structures and hyperparameter configurations of each algorithm corresponding to Table 1 are as follows.

Table 3: ASPC hyperparameters.

Hyperparameter		Value
TD3+BC hyperparameters	Optimizer	Adam (Kingma 2014)
	Critic learning rate	3e-4
	Actor learning rate	3e-4
	Mini-batch size	256
	Discount factor	0.99
	Target update rate	5e-3
	Policy noise	0.2
	Policy noise clipping	(-0.5, 0.5)
Architecture	Policy update frequency	2
	Critic hidden dim	256
	Critic hidden layers	3
	Critic activation function	ReLU
	Critic LayerNorm	True
	Actor hidden dim	256
	Actor hidden layers	2
	Actor activation function	ReLU
ASPC hyperparameters	Initial α	2.5
	α learning rate	2e-3
	α learning rate decay	Exponential
	α update interval	10
	EMA smoothing factor	0.995

Table 4: TD3+BC hyperparameters.

Hyperparameter		Value
TD3+BC hyperparameters	Optimizer	Adam (Kingma 2014)
	Critic learning rate	3e-4
	Actor learning rate	3e-4
	Mini-batch size	256
	Discount factor	0.99
	Target update rate	5e-3
	Policy noise	0.2
	Policy noise clipping	(-0.5, 0.5)
Architecture	Policy update frequency	2
	α	2.5
	Critic hidden dim	256
	Critic hidden layers	3
	Critic activation function	ReLU
	Critic LayerNorm	True
	Actor hidden dim	256
	Actor hidden layers	2
ASPC hyperparameters	Actor activation function	ReLU

Table 5: wPC hyperparameters.

Hyperparameter		Value
wPC hyperparameters	Optimizer	Adam (Kingma 2014)
	Critic learning rate	3e-4
	Actor learning rate	3e-4
	Value learning rate	3e-4
	Mini-batch size	256
	Discount factor	0.99
	Target update rate	5e-3
	Policy noise	0.1
	Policy noise clipping	(-0.5, 0.5)
	Policy update frequency	2
Architecture	α	2.5
	Critic hidden dim	256
	Critic hidden layers	3
	Critic activation function	ReLU
	Critic LayerNorm	True
	Actor hidden dim	256
	Actor hidden layers	2
	Actor activation function	ReLU

Table 6: A2PR hyperparameters.

Hyper-parameters		Value
TD3+BC hyperparameters	Optimizer	Adam (Kingma 2014)
	Critic learning rate	3e-4
	Actor learning rate	3e-4
	Mini-batch size	256
	Discount factor	0.99
	Target update rate τ	5e-3
	Policy noise	0.2
	Policy noise clipping	(-0.5, 0.5)
Architecture	Policy update frequency	2
	α	2.5
	Q-Critic hidden dim	256
	Q-Critic hidden layers	3
	Q-Critic Activation function	ReLU
	V-Critic hidden dim	256
	V-Critic hidden layers	3
	V-Critic Activation function	ReLU
A2PR hyperparameters	Actor hidden dim	256
	Actor hidden layers	2
	Actor Activation function	ReLU
	Normalized state	True
ϵ_A	w_1, w_2	0
		1.0

Table 7: IQL hyperparameters.

Hyperparameter		Value
IQL hyperparameters	Optimizer	Adam (Kingma 2014)
	Critic learning rate	3e-4
	Actor learning rate	3e-4
	Value learning rate	3e-4
	Mini-batch size	256
	Discount factor	0.99
	Target update rate	5e-3
	Learning rate decay	Cosine
Architecture	Critic hidden dim	256
	Critic hidden layers	2
	Critic activation function	ReLU
	Actor hidden dim	256
	Actor hidden layers	2
	Actor activation function	ReLU
	Value hidden dim	256
	Value hidden layers	2
	Value activation function	ReLU

Table 8: IQL’s best hyperparameters used in D4RL benchmark.

Task Name	β	IQL τ	Deterministic policy
halfcheetah-random	3.0	0.95	False
halfcheetah-medium	3.0	0.95	False
halfcheetah-expert	6.0	0.9	False
halfcheetah-medium-expert	3.0	0.7	False
halfcheetah-medium-replay	3.0	0.95	False
halfcheetah-full-replay	1.0	0.7	False
hopper-random	1.0	0.95	False
hopper-medium	3.0	0.7	True
hopper-expert	3.0	0.5	False
hopper-medium-expert	6.0	0.7	False
hopper-medium-replay	6.0	0.7	True
hopper-full-replay	10.0	0.9	False
walker2d-random	0.5	0.9	False
walker2d-medium	6.0	0.5	False
walker2d-expert	6.0	0.9	False
walker2d-medium-expert	1.0	0.5	False
walker2d-medium-replay	0.5	0.7	False
walker2d-full-replay	1.0	0.7	False
maze2d-umaze	3.0	0.7	False
maze2d-medium	3.0	0.7	False
maze2d-large	3.0	0.7	False
antmaze-umaze	10.0	0.7	False
antmaze-umaze-diverse	10.0	0.95	False
antmaze-medium-play	6.0	0.9	False
antmaze-medium-diverse	6.0	0.9	False
antmaze-large-play	10.0	0.9	False
antmaze-large-diverse	6.0	0.9	False
pen-human	1.0	0.95	False
pen-cloned	10.0	0.9	False
pen-expert	10.0	0.8	False
door-human	0.5	0.9	False
door-cloned	6.0	0.7	False
door-expert	0.5	0.7	False
hammer-human	3.0	0.9	False
hammer-cloned	6.0	0.7	False
hammer-expert	0.5	0.95	False
relocate-human	1.0	0.95	False
relocate-cloned	6.0	0.9	False
relocate-expert	10.0	0.9	False

Table 9: ReBRAC hyperparameters.

Hyperparameter		Value
ReBRAC hyperparameters	Optimizer	Adam (Kingma 2014)
	Mini-batch size	1024 on Gym-MuJoCo, 256 on others
	Learning rate	1e-3 on Gym-MuJoCo, 1e-4 on AntMaze
	Discount factor γ	0.999 on AntMaze, 0.99 on others
	Target update rate τ	5e-3
Architecture	Hidden dim (all networks)	256
	Hidden layers (all networks)	3
	Activation function	ReLU
	Critic LayerNorm	True

Table 10: ReBRAC’s best hyperparameters used in D4RL benchmark.

Task Name	β_1 (actor)	β_2 (critic)
halfcheetah-random	0.001	0.1
halfcheetah-medium	0.001	0.01
halfcheetah-expert	0.01	0.01
halfcheetah-medium-expert	0.01	0.1
halfcheetah-medium-replay	0.01	0.001
halfcheetah-full-replay	0.001	0.1
hopper-random	0.001	0.01
hopper-medium	0.01	0.001
hopper-expert	0.1	0.001
hopper-medium-expert	0.1	0.01
hopper-medium-replay	0.05	0.5
hopper-full-replay	0.01	0.01
walker2d-random	0.01	0.0
walker2d-medium	0.05	0.1
walker2d-expert	0.01	0.5
walker2d-medium-expert	0.01	0.01
walker2d-medium-replay	0.05	0.01
walker2d-full-replay	0.01	0.01
maze2d-umaze	0.003	0.001
maze2d-medium	0.003	0.001
maze2d-large	0.003	0.001
antmaze-umaze	0.003	0.002
antmaze-umaze-diverse	0.003	0.001
antmaze-medium-play	0.001	0.0005
antmaze-medium-diverse	0.001	0.0
antmaze-large-play	0.002	0.001
antmaze-large-diverse	0.002	0.002
pen-human	0.1	0.5
pen-cloned	0.05	0.5
pen-expert	0.01	0.01
door-human	0.1	0.1
door-cloned	0.01	0.1
door-expert	0.05	0.01
hammer-human	0.01	0.5
hammer-cloned	0.1	0.5
hammer-expert	0.01	0.01
relocate-human	0.1	0.01
relocate-cloned	0.1	0.01
relocate-expert	0.05	0.01

C Learning Curves

C.1 α Curves

Figure 8 plots the α learning curves for all 39 datasets. The curves show that our algorithm (i) drives α toward distinct optima across tasks and (ii) merely modulates its step size and pace when the dataset quality changes within the same task. This dual behaviour highlights the method’s adaptability to both task differences and data-quality variations.

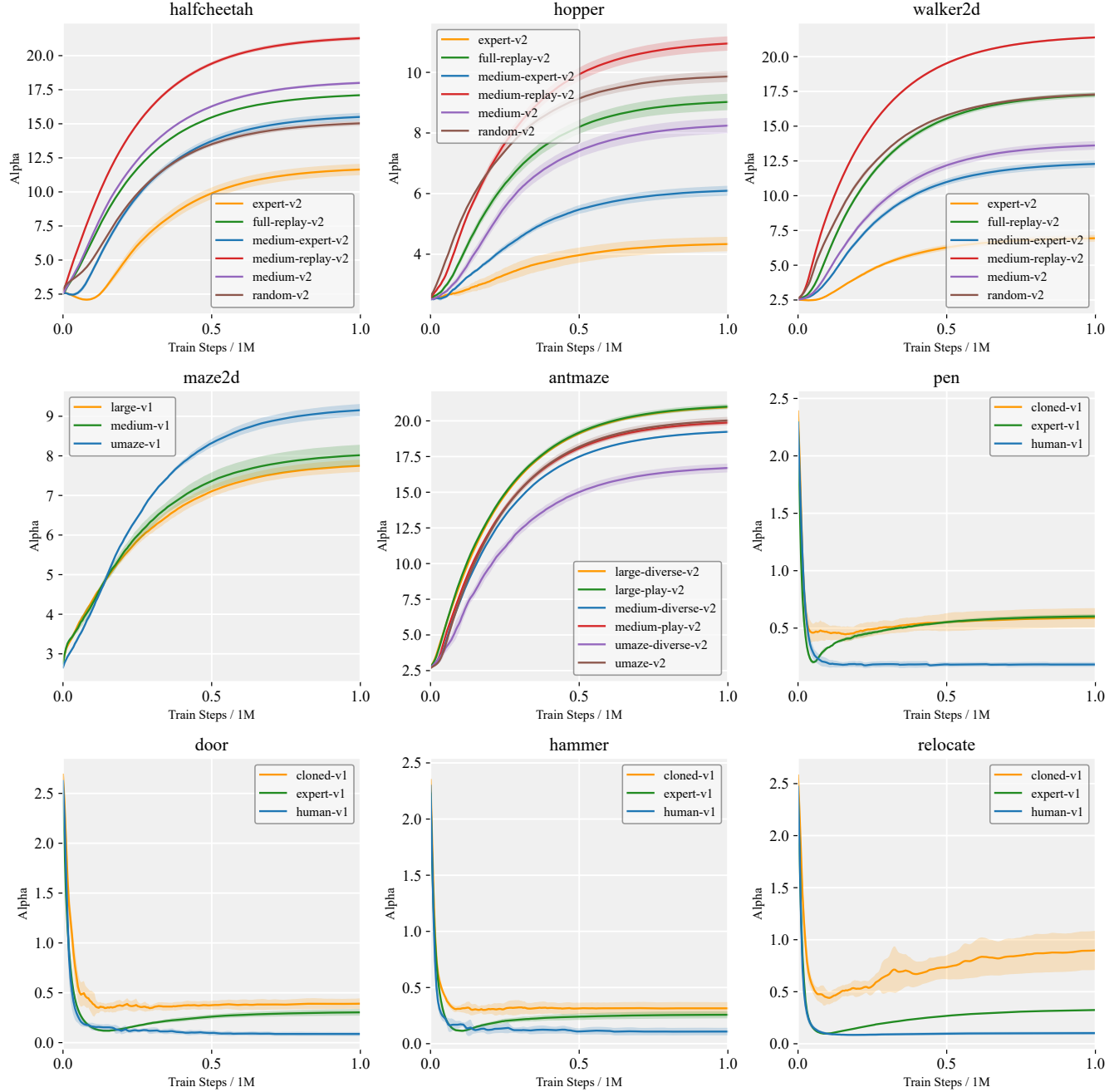


Figure 8: Learning curves of α for nine tasks across 39 datasets.

C.2 Performance Curves

Figure 9 shows the learning curves of all four algorithms on the 39 D4RL datasets. ASPC rises much more rapidly than the baselines, typically within the first 0.2–0.3 M environment steps, and surpasses them long before the others stabilize. Its final normalized scores are almost always the highest (or very close to the highest) across all task families, maintaining a clear margin where the competing methods usually plateau. Moreover, the shaded regions (mean \pm 1

s.d. over four seeds) remain consistently narrow for ASPC, and its curves show no late-stage collapses, pointing to lower variance and steadier adaptation across widely varying task dynamics and data quality. Overall, the figure suggests that ASPC combines greater sample efficiency, stronger ultimate performance, and more reliable behavior than the other approaches.

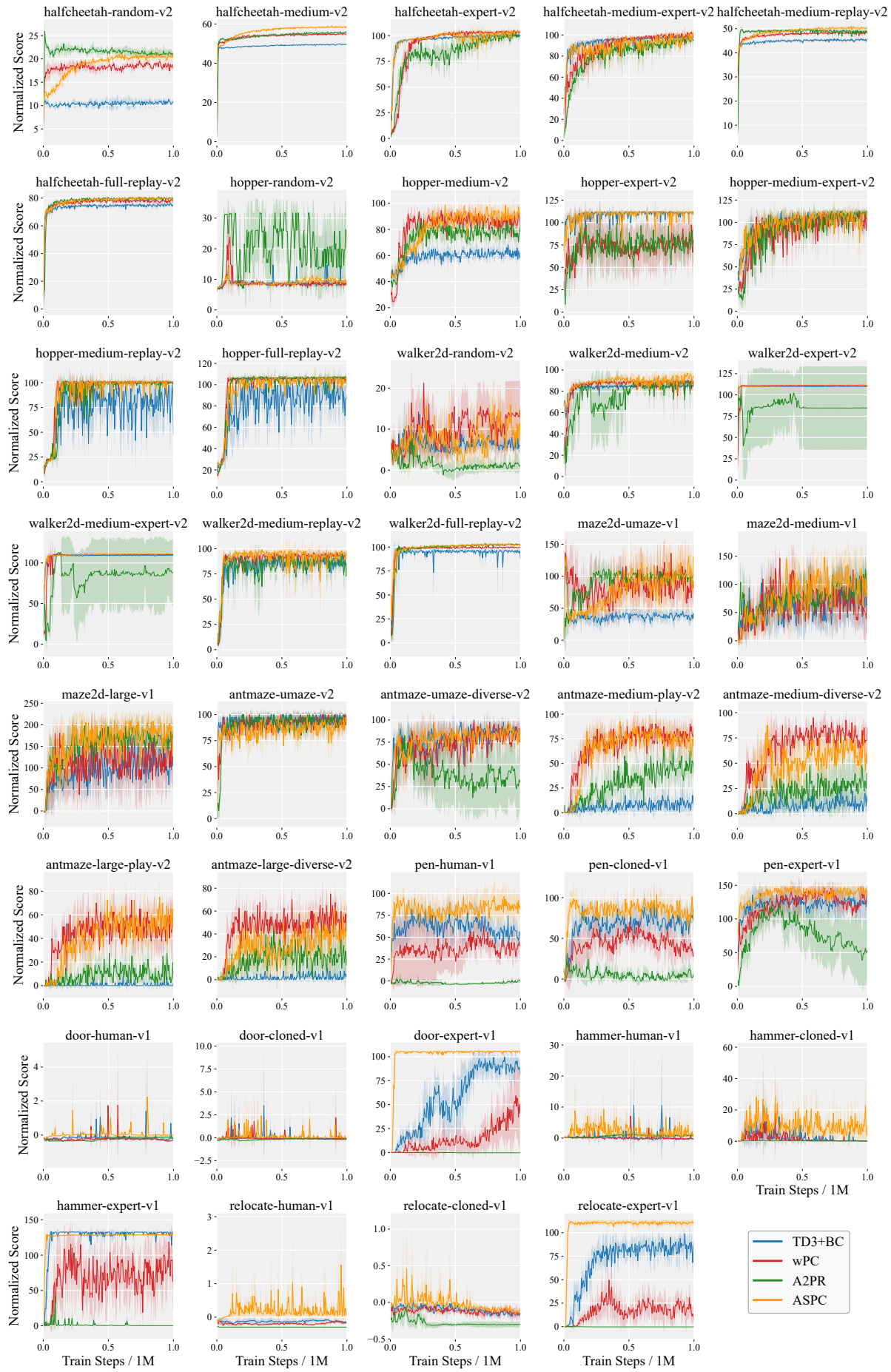


Figure 9: Learning curves comparing the performance of ASPC against other baselines.